In Silico and *in Vitro* Strategies against MCF-7 Cells using Fluorinated Xanthone Derivatives

Salsabiilaa Mohd Razib[1], Pavithren Devakrishnan[1], Nadiah Mad Nasir[1]*, Johnson Stanslas[2], Fatin Farhana Baharuddin[1] and Muhammad Kumayl Abdulwahab[3]

[1]Department of Chemistry, Faculty of Sciences, University Putra Malaysia, Selangor, Malaysia
[2]Department of Medicine, Faculty of Medicine and Health Sciences, Universiti Putra Malaysia
[3]Department of Chemistry, Faculty of Science, Universiti Malaya, Kuala Lumpur Malaysia
*Corresponding author (e-mail: nadiahmadnasir@upm.edu.my)

Six xanthone derivatives were successfully synthesized, including three newly fluorinated xanthones (**4-6**). The binding affinities of compounds with receptors associated with breast cancer (3EQM) were assessed, and compound **6** showed the highest binding energy with -9.8 kcal/mol. A QSAR (Quantitative Structure–Activity Relationship) model using seven descriptors was developed to predict anticancer activity, and it found that binding affinity played a key role in identifying strong anticancer inhibitors. Molecular dynamics simulations demonstrated stability and provided details on ligand-receptor interactions. Compound **6** inhibited the MCF-7 cell line at 10 μM with IC_{50} values of 92.24 ± 1.04 %, while causing minimal harm in Beas-2B cells (normal lung cells). As compound **6** is a non-toxic compound, its derivatives should be investigated for further bioactivities.

Keywords: synthesis, QSAR, cancer, xanthone, molecular docking, molecular dynamic

Received: February 2025; Accepted: April 2025

Cancers are characterized by the relentless division of cells, leading to the development of solid tumours and the potential for metastasis. In 2022, there were an estimated 20 million new cancer cases and 9.7 million deaths due to cancer, which stands as the second primary contributor to mortality [1–3]. In 2001, the Seidman group reported a potent nucleoside analogue, gemcitabine, with significant anticancer activities including prostate, cervical, oestrogen-dependent breast, and non-small cell lung cancer [4]. This chemotherapy medication, gemcitabine (Food & Drug Administration approved drug, application number: 200795Orig1s000) [5], contains fluorine in its structure. Fluorinated organic compounds have been widely used in agricultural, medicinal, and materials applications [6]. The inclusion of fluorine or fluorinated moieties can frequently improve the lipophilicity, metabolic stability, and bioavailability of their parent molecules [7].

Research into new anticancer drugs from natural sources and synthetic methods is still being conducted, and to date, more than 85 % of bioactive compounds discovered recently have consisted of heterocyclic structures [8]. Among the heterocyclic compounds, hundreds of xanthone derivatives have been isolated, synthesized, and evaluated as anticancer agents [9]. In 2020, Zhang and group reported that the most abundant xanthone isolated from the pericarps of mangosteens, α-mangostin, exhibited a potent anti-HCC (Hepatocellular carcinoma) effect by blocking the STAT3 (Signal transducer and activator of transcription 3) signalling pathway via suppression of the degradation of SHP1 (Protein Tyrosine Phosphatase) induced by the ubiquitin–proteasome pathway. Overly activated STAT3 promotes the expression of genes that involve proliferation, anti-apoptosis, metastasis and inflammation, which contribute to malignant transformation and tumour production [10]. Since STAT3 promotes cancer progression by regulating genes involved in cell growth, survival, and immune evasion, inhibiting the STAT3 pathway or restoring SHP1 activity is important in helping to suppress tumours, strengthen immune responses, and improve chemotherapy effectiveness [10].

Therefore, Zhang's findings suggest that xanthone (α-mangostin) is a promising lead compound for cancer chemotherapy [10]. Halogenated xanthones are molecules with one or more halogen atoms placed in the aromatic moiety of the xanthone chromophore. Present in both natural products and synthetic compounds, they constitute important structural motifs in medicinal chemistry and show biological activities [11]. However, no studies have been reported on the activity of fluorinated xanthones against cancer, particularly breast cancer.

Based on the Parasrampuria group's report [12], the major reasons for failure in the late stage of drug development can be classified into two main groups: (1) Unavoidable failures due to inadequate scientific advances, such as the lack of predictive translational preclinical *in vitro* and in vivo models for safety and efficacy, and (2) Avoidable failures that can

be mitigated through scientific rigour, curiosity, and discipline, such as suboptimal study designs with inadequate controls in Phase 2 (experiments), leading to false-positive outcomes that cannot be replicated in Phase 3 (clinical trials). In order to improve success rates and reduce downtime, several computational tools have been integrated as supporting tools. In silico technologies have been successful in identifying anticancer medications [13]. A well-known in silico method for learning pertinent information about the primary physiochemical parameters necessary for the excellent potency of bioactive compounds is quantitative structure-activity relationship (QSAR) modelling. QSAR modelling is frequently used to direct structural change and compound design, resulting in new derivatives with better bioactivity and suitable pharmacophore properties [14–16].

The objective of this research was to modify the major structures of xanthone with a fluorine variety of substituents (**Scheme 1**), which will significantly impact the xanthonoids' inhibitory effect and will focus on oestrogen-dependent breast cancer [16,17]. The binding affinity values, as well as the chemical structures of the compounds, were used as input data sets for QSAR model construction using ChemMaster 1.1 software and a total of seven descriptors were used to identify crucial chemical characteristics, which would be useful in order to achieve future success in the discovery of new fluorinated xanthone derivatives as anticancer agents [14–16].

To elucidate the mechanism of inhibition by derivatives, intermolecular interactions between the compounds and the target macromolecules were identified using the Lipinski rule of 5 [18]. All compounds (**1**-**6**) were docked to determine the interactions between ligands and 3EQM (oestrogen-dependent breast cancer) receptors associated with the cancers outlined in this study [19]. Compounds with higher binding affinity to the receptor were further analyzed for their interactions, and finally, all derivatives were experimentally evaluated using the MTT (3-(4,5-dimethylthiazol-2-yl)-2,5-diphenyltetrazolium bromide) cell viability assay to measure their inhibitory effects.

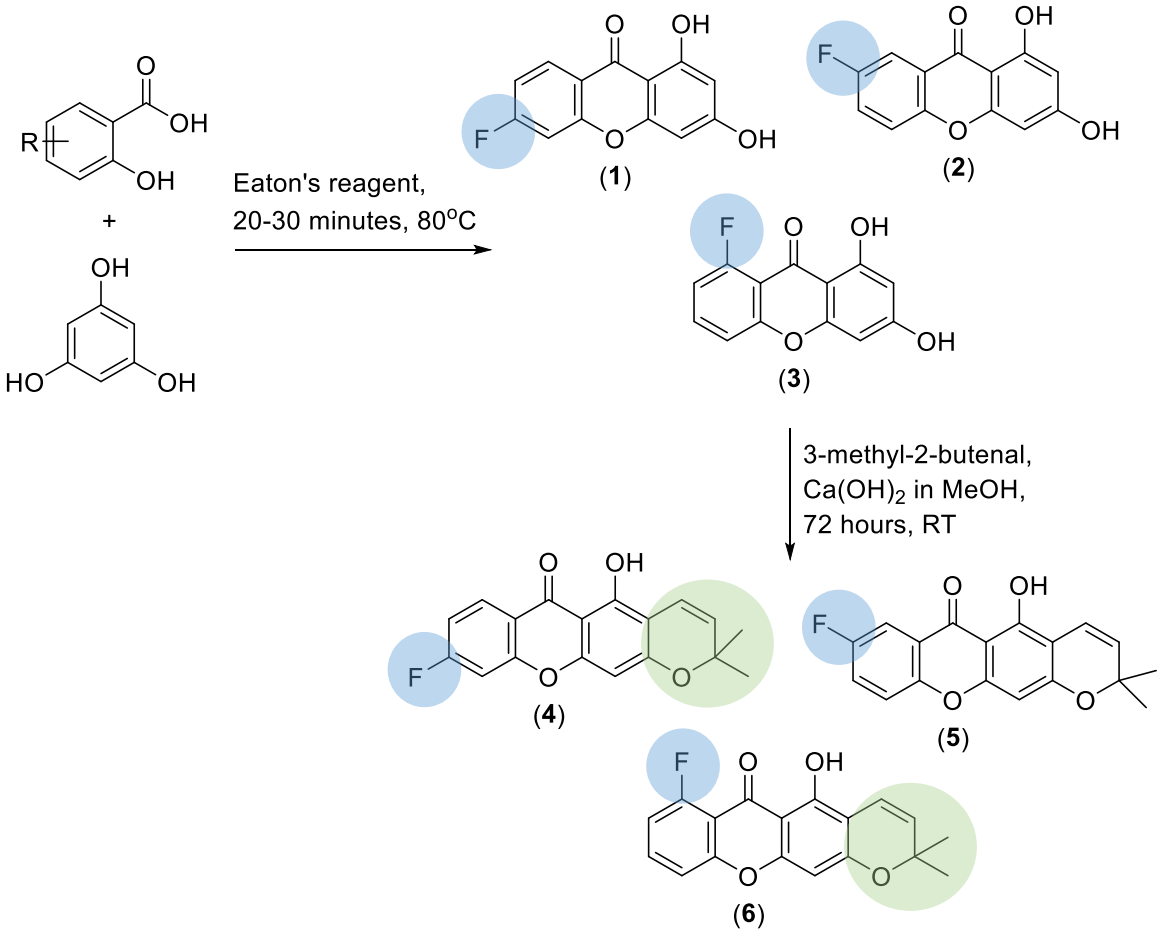

Scheme 1. The stepwise chemical synthesis of the fluorinated xanthones (**1**-**6**). Identification of the structures of **1**-**6** was accomplished through spectral data analysis (see supporting documents**)**, including Fourier Transform Infrared Spectroscopy (FTIR), Nuclear Magnetic Resonance Spectroscopy (1D and 2D NMR), and Direct Infusion Mass Spectrometry (DIMS) techniques.

EXPERIMENTAL

Chemicals and Materials

All reagents and solvents used in this study were commercially sourced from Sigma Aldrich. Key chemical reagents included phloroglucinol, various fluorosalicylic derivatives, 3-methyl-2-butenal, calcium hydroxide, hydrochloric acid, methanol, hexane, ethyl acetate, and chloroform. Product purification was conducted using Kieselgel 60, and thin-layer chromatography (TLC) was performed on silica gel-coated aluminium sheets, which were visualized under ultraviolet light at both short (254 nm) and long (365 nm) wavelengths. The ^{1}H-NMR, ^{13}C-NMR, and 2D NMR [HSQC (Heteronuclear Single Quantum Coherence) and HMBC (Heteronuclear Multiple Bond Correlation)] spectra were obtained at 500 MHz (^{1}H) and 125 MHz (^{13}C) with a Varian 500 MHz instrument. The NMR spectra were recorded in deuterated solvents, with chemical shifts given in ppm relative to TMS. Next, the functional groups were analysed using FTIR [Attenuated Total Reflectance (ATR) technique], with spectra recorded from 650 cm^{-1} to 4000 cm^{-1}. The molecular weights of the synthesized products were determined using the direct-injection (DIMS) technique. The melting points of the synthesized compounds were obtained using a Fisher-Johns melting point apparatus.

Characterization Methods

The process of generating xanthone derivatives involved combining various salicylic acids with phloroglucinol, followed by the addition of Eaton's reagent as a coupling agent. The mixture was then heated under reflux at 80 °C for 20-30 minutes (**Scheme 1**). The resulting synthesized products (**1-3**) were purified via column chromatography on silica gel, using polarity as the elution method. Next, the purified compounds **1-3** underwent cyclization to form derivatives **4-6** (**Scheme 1**). To synthesize the prenylated xanthone derivatives (**4-6**), 3-methyl-2-butenal was introduced to the previously synthesized xanthone along with calcium hydroxide [$Ca(OH)_2$] in methanol (MeOH) and stirred at ambient temperature for 72 hours. The resulting crude products were then purified via column chromatography on silica gel, utilizing polarity as the elution method [20, 21].

Experimental Data (1-6)

Synthesis of 6-fluoro-1,3-dihydroxy-9H-xanthen-9-one (1)

Orange solid; 87.87 % yield; m.p. 264.20 °C; [Eluent: Hexane: Ethyl Acetate (9:1)]; ^{1}H-NMR (500 MHz, dimethyl sulfoxide-d_6) δ: 6.21 (d, 1H, *J* = 2.10 Hz, H-2), 6.38 (d, 1H, *J* = 2.10 Hz, H-4), 7.33 (td, 1H, *J* = 2.40, 8.70 Hz, H-7), 7.54 (dd, 1H, *J* = 2.40, 9.80 Hz, H-5), 8.17 (dd, 1H, *J* = 6.50, 8.70 Hz, H-8), 12.70 (s, 1-OH); ^{13}C NMR (125 MHz, dimethyl sulfoxide-d_6) δ: 94.2 (C-4), 98.5 (C-2), 101.9 (C-9a), 104.6 & 104.8 (C-5), 112.9 & 113.1 (C-7), 117.1 (C-8a), 128.1 & 128.2 (C-8), 156.7 (C-10a), 157.5 (C-4a), 162.9 (C-3), 166.0 (C-1), 167.0 (C-6), 178.9 (C-9); IR (ATR): 3523.00 (OH alcohol), 2920.00 (OH alcohol), 2100.00-2000.00 (CH aromatic, overtone), 1604.00 (C=O), 1439.00 (C-F), 1260.00 (C-O), 774.00 (oop CH aromatic) cm^{-1}; DI-MS m/z calcd for $C_{13}H_7FO_4$ [M]+ 246.19, found 246.05, 218.10, 189.10, 123.00. [22,23].

Synthesis of 7-fluoro-1,3-dihydroxy-9H-xanthen-9-one (2)

Light yellow solid; 40.31 % yield; m.p. 254.30 °C; [Eluent: Hexane: Ethyl Acetate (90:10)]; ^{1}H-NMR (500 MHz, acetone-d6) δ 6.25 (d, 1H, *J* = 2.10 Hz, H-2), 6.40 (d, 1H, *J* = 2.10 Hz, H-4), 7.57 (dd, 1H, *J* = 4.25, 9.15 Hz, H-5), 7.62 (td, 1H, *J* = 3.05, 9.15 Hz, H-6), 7.77 (dd, 1H, *J* = 3.05, 8.30 Hz, H-8), 10.06 (s, 3-OH), 12.70 (s, 1-OH); ^{13}C-NMR (125 MHz, acetone-d_6) δ 94.9 (C-4), 99.2 (C-2), 103.4 (C-8a), 110.8 & 111.0 (C-8), 120.9 & 121.0 (C-8), 123.9 & 124.1 (C-6), 153.1 (C-10a), 158.6 (C-9a), 158.8 (C-4a), 160.6 (C-7), 164.5 (C-3), 166.8 (C-1), 180.4 (C-9); IR (ATR): 3335.05 (OH alcohol), 2926.2 (OH alcohol), 2026.49-1919.41 (CH aromatic, overtone), 1615.88 (C=O), 1480.04 (C-F), 1268.84 (C-O), 827.48 (oop CH aromatic) cm^{-1}; DI-MS m/z calcd for $C_{13}H_7FO_4$ [M]+ 246.19, found 246.05, 218.10, 189.05, 123.00. [22,23].

Synthesis of 8-fluoro-1,3-dihydroxy-9H-xanthen-9-one (3)

Light yellow solid; 39.28 % yield; m.p: 296.70 °C; [Eluent: Hexane: Ethyl Acetate (90:10)]; ^{1}H-NMR (500 MHz, methanol-d4) δ 6.19 (d, 1H, *J* = 2.15 Hz, H-2), 6.32 (d, 1H, *J* = 2.15 Hz, H-4), 7.08 (dd, 1H, *J* = 2.75, 8.30 Hz, H-5), 7.30 (d, 1H, *J* = 8.30 Hz, H-6), 7.73 (dd, 1H, *J* = 2.75, 8.30 Hz, H-7); ^{13}C-NMR (125 MHz, methanol-d4) δ 94.9 (C-4), 99.5 (C-5), 111.4 (C-9a), 112.0 & 112.2 (C-7), 114.7 & 114.8 (C-5), 118.6 (C-8a), 136.6 & 136.8 (C-6), 158.7 (C-10a), 161.5 (C-4a), 164.9 (C-8), 167.5 (C-3), 167.5 (C-1), 180.8 (C-1); IR (ATR): 3358.93 (OH alcohol), 2969.81 (OH alcohol), 2000.00 (CH aromatic, overtone), 1619.69 (C=O), 1263.22 (C-O), 1263.22 (C-F), 813.23 (oop CH aromatic) cm^{-1}; DI-MS m/z calcd for $C_{13}H_7FO_4$ [M]+ 246.19, found 246.05, 218.10, 189.05, 123.00 [22,23].

Synthesis of 6-fluoro-1-hydroxy-6',6'-dimethylpyrano [3,2-b] xanthen-6(2H)-one (4)

Yellow crystals; 48.00 % yield; m.p 176.90 °C; [Eluent: Hexane: Ethyl Acetate (95:5)]; ^{1}H-NMR (500 MHz, chloroform-d) δ 1.47 (s, 6H, 2-CH_3, H-4' & H-5'), 5.59 (d, 1H, *J* = 10.05 Hz, H-2'), 6.31 (s, 1H, H-4), 6.69 (d, 1H, *J* = 10.05 Hz, H-1'), 7.04 (d, 1H, *J* = 2.35 Hz, H-5), 7.07 (dd, 1H, *J* = 2.35, 8.25 Hz, H-7), 8.21 (dd, 1H, *J* = 2.35, 8.25 Hz, H-8), 13.00 (s, 1H, 1-OH); ^{13}C-NMR (125 MHz chloroform-d) δ 28.51 (2-CH3, C-4' & C-5'), 78.5 (C-3'), 95.3 (C-4), 103.5 (C-9a), 104.4 &

104.6 (C-5), 105.0 (C-2), 112.7 & 112.9 (C-7), 115.4 (C-1'), 117.5 (C-8a), 127.8 (C-2'), 128.4 & 128.5 (C-8), 157.2 (C-10a), 157.8 (C-3), 161.0 (C-1), 165.6 (C-4a), 167.6 (C-6), 180.0 (C-9); IR (ATR): 3066.34 (OH alcohol), 2926.33 (OH alcohol), 2100-1910.25 (CH aromatic, overtone), 1616.76 (C=O), 1457.77 (CH methyl group), 1260.51 (C-O), 1160.06 (C-F), 813.30 (oop CH aromatic) cm^{-1}; DI-MS m/z calcd for $C_{18}H_{13}FO_4$ [M]+ 312.29, found 250.10, 221.10, 139.05, 125.05.

Synthesis of 7-fluoro-1-hydroxy-6',6'-dimethylpyrano [3,2-b] xanthen-6(2H)-one (5)

Bright yellow crystals; 39.00 % yield; m.p 165.70 °C; [Eluent: Hexane: Ethyl Acetate (98:2)]; ^{1}H-NMR (500 MHz, chloroform-d) δ 1.48 (s, 6H, 2-CH_3, H-4' & H-5'), 5.61 (d, 1H, *J* = 10.05 Hz , H-2'), 6.34 (s, 1H, H-4), 6.72 (d, 1H, *J* = 10.05 Hz), 7.41 (dd, 1H, *J* = 1.65, 8.25 Hz, H-5 & H-6), 7.86 (dt, 1H, *J* = 1.65, 8.25 Hz, H-8), 12.96 (s, 1H, 1-OH); ^{13}C-NMR (125 MHz chloroform-d) δ 28.6 (2-CH3, C-4' & C-5'), 78.6 (C-3'), 95.2 (C-4), 103.4 (C-9a), 104.8 (C-2), 110.7 & 110.9 (C-8), 115.4 (C-1'), 119.6 & 119.7 (C-5), 122.8 & 123.0 (C-6), 127.8 (C-2'), 152.2 (C-10a), 157.2 (C-1), 157.6 (C-4a), 159.8 (C-7), 161.2 (C-3), 180.0 (C-9); IR (ATR): 3074.52 (OH alcohol), 2970.77 (OH alcohol), 2300-1897.59 (CH aromatic, overtone), 1648.96 (C=O), 1475.19 (CH methyl group), 1260.15 (C-O), 1129.49 (C-F), 821.75 (oop CH aromatic) cm^{-1}; DI-MS m/z calcd for $C_{18}H_{13}FO_4$ [M]+ 312.29, found 312.1, 297.15, 148.5.

Synthesis of 8-fluoro-1-hydroxy-6',6'-dimethylpyrano [3,2-b] xanthen-6(2H)-one (6)

Yellow crystals; 20.34 % yield; m.p 168.20 °C; [Eluent: Hexane: Ethyl Acetate (95:5)]; ^{1}H-NMR (500 MHz, acetone-d6) δ 1.48 (s, 6H, 2-CH_3, H-4' & H-5'), 5.60 (d, 1H, *J* = 10.05 Hz, H-2'), 6.31 (s, 1H, H-4), 6.72 (d, 1H, *J* = 10.05 Hz, H-1'), 7.01 (dd, 1H, *J* = 2.75, 8.55 Hz, H-7), 7.22 (d, 1H, *J* = 8.55 Hz, H-6), 7.62 (td, 1H, *J* = 2.75, 8.55 Hz, H-5), 13.16 (s, 1H, 1-OH); ^{13}C-NMR (125 MHz acetone-d6) δ 28.6 (2-CH3, C-4' & C-5'), 78.6 (C-3'), 95.0 (C-4), 104.1 (C-9a), 105.1 (C-2), 111.2 & 111.3 (C-7), 113.7 & 113.7 (C-6), 115.5 (C-1'), 127.8 (C-2'), 135.0 & 135.1 (C-5), 156.5 (C-4a), 156.9 & 157.0 (C-10a), 158.0 (C-3), 160.4 (C-8a), 161.1 (C-1), 162.5 (C-8), 180.0 (C-9); IR (ATR): 3453.50 (OH alcohol), 2968.51 (OH alcohol), 2081.16-1940.92 (CH aromatic, overtone), 1614.50 (C=O), 1477.11 (CH methyl group), 1213.86 (C-O), 1138.41 (C-F), 820.70 (oop CH aromatic) cm^{-1}; DI-MS m/z calcd for $C_{18}H_{13}FO_4$ [M]+ 312.29, found 312.1, 297.15, 148.5.

Molecular Docking

The crystal structures employed in this research comprised 3EQM (oestrogen-dependent breast cancer) protein [24–26]. The molecular configuration for the protein was obtained from the RCSB Protein Data Bank (http://www.rcsb.org/). The possible binding interactions of the synthesized compounds with the protein were investigated using molecular docking analysis. This study used the AutoDockTools 1.5.4 (https://mgltools.scripps.edu) and AutoDock Vina (https://vina.scripps.edu) programs. The crystal structure was prepared for molecular docking using the BIOVIA Discovery Studio Visualizer. All water molecules were removed, and the resulting structure was stored in .pdbqt format [27]. The removal of water molecules from the crystal structure was performed to simplify the computational procedure and ensure a clear binding location, thereby improving the precision and efficiency of molecular docking simulations [28]. The final phase required adding hydrogen atoms to facilitate hydrogen bond formation, ensuring complete and accurate molecular structures for docking simulations, which improved the reliability of the results obtained using AutoDockTools 1.5.4 [29]. The Avogadro software [30] was used to generate 3D structures of the synthesized molecules. An energy optimization tool within the software was subsequently used to stabilize the 3D structures of the ligands, preparing them for molecular docking analysis [31]. All ligands were then saved in .pdbqt file format for molecular docking.

AutoDock Vina was employed to dock optimized ligand molecules into an improved protein model. This approach aimed to identify the optimal ligand conformations within the binding sites of the target macromolecules and calculate the affinity energy of the interactions. The protein structure was initially loaded, and the active site was identified using the native location of the co-crystallized ligand to determine the binding pocket of the target receptor [32, 33]. The docking grid parameters for the receptor are shown in Table 1. A grid spacing of 1.0 Å was applied for all systems. The analogues were then processed using Biovia Discovery Studio Visualizer, which generated lists of interactions and enhanced ligand-protein residue visuals in both 2D and 3D. After preparing the separated co-crystallized ligands using the same standardized procedure, AutoDock Vina was used to re-dock them into the corresponding protein binding sites. To validate the docking technique, the docked position was overlaid on the original pose, and the Root Mean Square Deviation (RMSD) for all proteins was calculated.

Table 1. The docking grid parameters for the receptor 3EQM.

Crystal structure (receptor)	Grid Box					
	x-axis	y-axis	z-axis	Centre-x	Centre-y	Centre-z
3EQM	54.00	66.00	46.00	85.14	53.00	49.09

QSAR Studies

Using molecular docking data, fluorinated xanthone derivatives were utilized to build QSAR models. The training set data were represented by red crosses, while the test set data were represented by blue crosses. The QSAR models were constructed using ChemMaster 1.1 software, and a total of seven descriptors were used to generate the model: Aromatic heavy atoms, Hydrogen-bond (H-bond) acceptors, Hydrogen-bond (H-bond) donors, Rotatable bonds, Molecular weight (MW), LogP, and Lipinski violations. The two-dimensional (2D) QSAR model was validated using the coefficient of determination (R^2), root mean square error (RMSE), mean absolute error (MAE), and predictive relevance (Q2) values [15].

Molecular Dynamics

The model for the aromatase receptor was obtained from the Protein Data Bank (PDB ID: 3EQM) [28]. The protonation state of ionizable protein side chains was assigned at pH 7. The conformation of compound **6**, obtained from the molecular docking experiment, was used as the ligand. Each system was solvated in a periodic box using the TIP3P (transferable intermolecular potential with 3 points) water model, maintaining a 12 Å distance from the protein surface. Sodium ions were added to neutralize the system using the tLeap module, implemented in the AMBER 22 package [34]. The topology and initial coordinates generated by tLeap were gradually minimized and structurally relaxed by harmonic potentials using the SANDER program. The system was heated to 300 K for 200 ps and then simulated for 50 ns to evaluate ligand-binding stability over the MD trajectory. The interaction energy of the trajectory was calculated using the MMPBSA (Molecular Mechanics Poisson-Boltzmann Surface Area) method [35]. Hydrogen bonding occupancy analysis was performed using the cpptraj program [36].

ADMET and Drug-likeness

In drug discovery, ADMET (absorption–distribution–metabolism–excretion–toxicity) studies are applied to analyse the pharmacological structure. In this study, a total of 20 parameters in ADMET data were generated using ADMETlab 2.0 [37], a comprehensive and precise online platform for predicting ADMET properties. Next, SwissADME [38], an online program, was used to estimate the drug-likeness and pharmacokinetics of the substances [39].

Bioassay

The growth-inhibitory potential of the derivatives on MCF-7 (human breast cancer) and Beas-2B (non-tumorigenic human lung epithelial) cell lines was determined using an MTT cell viability assay [33, 40]. The cell lines were seeded into each well of a 96-well microplate. The positive and negative controls used in this assay were gemcitabine and dimethyl sulfoxide (DMSO), respectively. The cells were incubated overnight at 37 °C with 5 % CO_2 to allow attachment to the wells before being treated with 10 µM concentrations of the derivatives. A 20 µL aliquot of each derivative was obtained from the stock solutions (100 mg mL^{-1} in DMSO) in RPMI 1640 medium and added into each well to achieve a final volume of 200 µL per well in the microtiter plate. The concentration of derivatives was tested in quadruplicate, and the control wells contained 200 µL of medium. The culture plates were incubated at 37 °C for 96 hours with 5 % (v/v) CO_2. After 96 hours of incubation, 50 µL of MTT solution (2 mg mL^{-1} in PBS (Phosphate-buffered saline)) was added to each well containing 200 µL of medium and incubated at 37 °C for 2-4 hours. Excess MTT was discarded, and 100 µL of DMSO was added to each well and gently shaken to dissolve the purple formazan crystals. The absorbance values of formazan, as a measure of viable cells, were determined at 590 nm using a microplate reader. The cell viability percentage was calculated using the following formula:

$$\%\ Cytotoxicity = \frac{Absorbance\ of\ the\ treated\ cells}{Absorbance\ of\ the\ control\ cells} \times 100$$

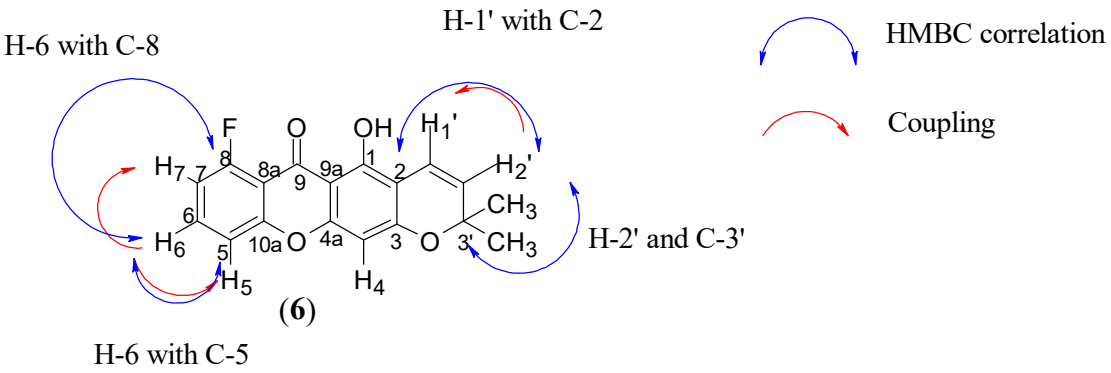

Figure 1. Structure of 8-fluoro-5-hydroxy-2,2-dimethylpyrano[3,2-b] xanthen-6(2H)-one (**6**).

RESULTS AND DISCUSSION

Chemistry

In this study, a total of six fluorinated xanthone derivatives were successfully synthesized and characterized. However, we will only discuss the active compound via the visual screening of compound **6**. The spectral data for the other five compounds (**1-5**) are provided in the experimental section and supporting documents (**Fig. S1–S27**). The new fluorinated xanthone, **6** (**Figure 1**), showed the highest binding affinity with the receptor (3EQM). The ^{1}H NMR spectrum indicated that there were two methyl groups at 1.48 ppm (s, 6H, 2CH_3), a hydroxyl group at 13.16 ppm (s, 1H, 1-OH) and six aromatic proton signals at 5.60 ppm (d, 1H, J = 10.05 Hz, H-2'), 6.31 ppm (s, 1H, H-4), 6.72 ppm (d, 1H, J = 10.05 Hz, H-1'), 7.01 ppm (dd, 1H, J = 2.75, 8.55 Hz, H-7), 7.22 ppm (d, 1H, J = 8.55 Hz, H-6), and 7.62 ppm (td, 1H, J = 2.75, 8.55 Hz, H-5). The pattern of ortho-coupling between H-4' and H-5' with a J value of 10.05 Hz and another ortho-coupling between H-6 and H-5; H-7 with a J value of 8.55 Hz was visible (see supporting documents).

The carbon signals of the representative compound **6** were unambiguously assigned using HMBC spectra. The presence of two methyl (C-4' & C-5') and quaternary carbons was confirmed by comparing the ^{13}C NMR spectrum to the reference (40). The ^{13}C NMR chemical shift measurements of **6** are listed in the supporting documents. The HMBC spectrum confirmed the structure of compound **6** with a ^{2}J correlation of H-6 to C-5 and a ^{3}J correlation of H-6 to C-8, whereas H-5' showed a ^{2}J correlation with C-3' and a ^{3}J correlation with C-2, as shown in **Figure 1** and the HMBC spectrum. The FT-IR spectrum and the molecular ion peak at m/z 312.10 $[M]^{+}$ generated from the DIMS analysis (supporting documents) were consistent with the expected molecular weight of $C_{18}H_{13}FO_4$.

Molecular Docking Analysis

Molecular docking was performed to determine the binding mechanism and assess the potential of compounds **1–6** and the standard drug (Gemcitabine**)** to serve as cancer inhibitors by examining the complex structures of potential receptors such as human placental aromatase cytochrome P450: breast cancer (PDB ID: 3EQM; 2.90 Å X-ray resolution). **Table 2** displays the computed RMSD values for the co-crystallized ligand pose vs the docked pose. Based on the findings of Devakrishnan et al (2025), docking solutions with RMSD values < 2.0 Å are in good agreement, whereas RMSD values ranging from 2.0 to 3.0 Å retain the desired orientation despite a change in the reference location [33]. As a result, appropriate RMSD values were obtained for the selected docking procedure, confirming its ability to replicate the original co-crystallized location.

The receptor was docked to discover the highest binding affinity of the compounds (**1-6**). Among them, the new fluorinated xanthone **6** exhibited the most substantial binding affinity for 3EQM at -9.8 kcal/mol (**Table 3**). Based on **Figure 2a**, ILE133, LEU477, and VAL370 were the residues interacting with compound **6** at the active site of the aromatase-androstenedione complex structure, 3EQM, via hydrophobic interactions. Compound **6** showed the best fit with the binding interactions of van der Waals, π-sigma, and π-alkyl bonds and acted as an aromatase inhibitor (AIs) that hindered the functioning of the enzyme aromatase. Aromatase, also known as oestrogen synthetase, belongs to the cytochrome P450 class of monooxygenases [42]. Notably, aromatase activity present in breast cells can act as a local source of oestrogen for tumour cells. Aromatase inhibition or deactivation reduces the proliferation of hormone receptor-positive breast cancer cells by lowering blood oestrogen levels [43].

Table 2. RMSD values for the molecular docking of 3EQM.

Receptors	RMSD (Å)
3EQM	2.892

Table 3. Highest binding affinities of compounds **1-6** with 3EQM receptors.

3EQM	
6: -9.8	**2: -8.3**
4: -9.7	**1: -8.3**
5: -8.6	**3: -7.7**
G: -7.2	

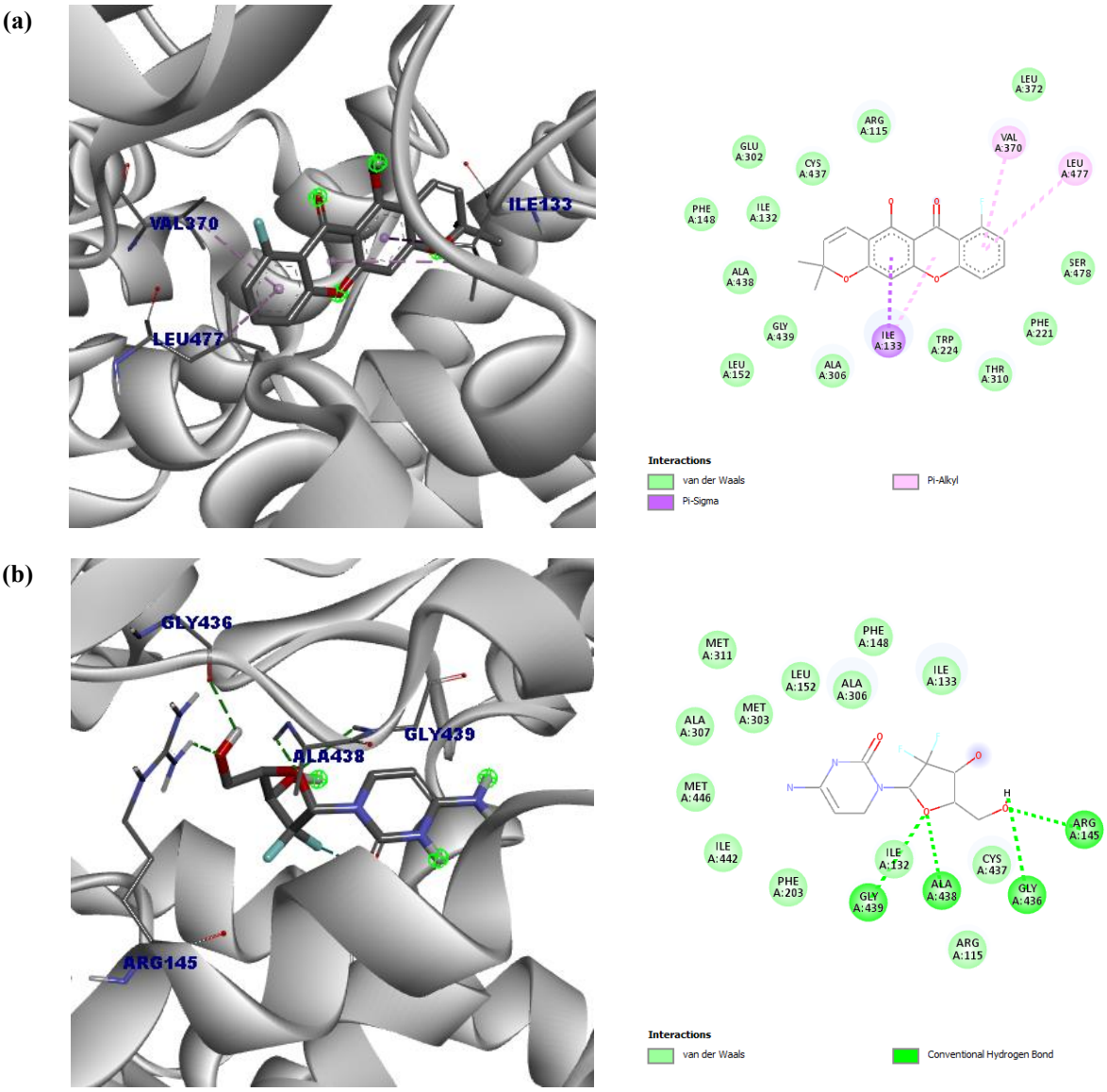

Figure 2. The molecular docking conformation and drug interactions with the active sites of human placental aromatase cytochrome P450 (PDB ID: 3EQM). The 3D and 2D docking representations of **(a)** compound **6** with 3EQM, and **(b)** gemcitabine with 3EQM.

Figure 2b shows the ligand-protein interactions of the FDA-approved drug, gemcitabine and the aromatase-androstenedione complex structure, 3EQM. Unlike compound **6**, gemcitabine only showed hydrogen bonding interactions with the protein, with a bond length of more than 2.00 Å. This is in agreement with the lower binding affinity of gemcitabine compared to compound **6**. Amino acid residues such as ARG145, ALA438, GLY436 and GLY439 were responsible for the interactions between the protein and gemcitabine, which were carbon hydrogen bonds, conventional hydrogen bonds and halogen (fluorine) interactions. Thus, molecular docking analysis indicates that compound **6** selectively demonstrated the strongest potential in inhibiting oestrogen-dependent breast cancer. A summary of the best fit binding affinity and key interactions of ligand and protein is given in **Table 4.**

QSAR Study

QSAR modelling was used to determine the connection between the structures of derivatives and their biological activities [13]. The properties of the compounds were conceptualized as a series of numbers known as descriptors. The bioactivity values were expressed as binding affinity, and the selected descriptors were tabulated in **Table 5**. Multiple linear regression (MLR) is a machine learning approach widely utilized in the field of drug development. As an input dataset for MLR QSAR modeling, a set of actual bioactivity values (binding affinity values) and selected descriptor values were prepared [47]. The model was then returned in the form of a linear equation representing the Y variable (bioactivity) as a function of numerous X variables (descriptors). The QSAR model was developed using the overall bioactivity data to develop a relationship between the xanthone derivatives and their anti-cancer activity, which will assist in the rational design of new active molecules. The coefficient of determination (R^2) (a statistical measure of how close the data are to the fitted regression line), root mean square error (RSME), mean absolute error (MAE) and predictive relevance (Q^2) values were used to assess the validity of the regression equation (**Table 6**).

In this study, the QSAR models (**Figure 3**) were built using compound **6** and seven descriptors (**Table 5**) with an R^2 value of 0.972, showing that the suggested model had enough statistical stability and validity despite the restricted number of molecules used to develop the model. The value of R^2 is a relative measure of a regression equation's quality of fit. Furthermore, this result was supported by the Q^2 value of 0.926. Q^2 determines if a model is predictive or not (> 0 is excellent). In other words, a good value for Q^2 is a value that is close to that of R^2. As the Q^2 value of 3EQM was close to the R^2 value, the QSAR model of 3EQM was the most significant for compound **6**. In conclusion, the QSAR study provided data for the structure-activity relationship investigation, as shown in **Figure 3**. These findings imply that fluorinated xanthone **6** might be an effective scaffold for the creation of novel and promising candidates in the treatment of breast cancer (3EQM).

Table 4. The interactions of gemcitabine and compound **6** with the aromatase-androstenedione complex structure (3EQM) as determined by molecular docking analysis.

	Gemcitabine		**Compound 6**	
Protein	**Binding Affinity (kcal/mol)**	**Key Interactions**	**Binding Affinity (kcal/mol)**	**Key Interactions**
3EQM	-7.2	GLY436, GLY439, ALA438, ARG145 (Conventional Hydrogen Bond), ALA306, ALA307, MET303, MET311, MET446, ILE132, ILE133, ILE442, PHE148, PHE203, LEU152, ARG115, CYS437 (van der Waals)	-9.8	LEU477, VAL370 (π-Alkyl), ILE133 (π -Sigma), PHE148, PHE221, ILE132, GLU302, CYS437, ARG115, LEU152, LEU 372, SER478, THR310, TRP224, ALA306, ALA438, GLY439 (van der Waals)

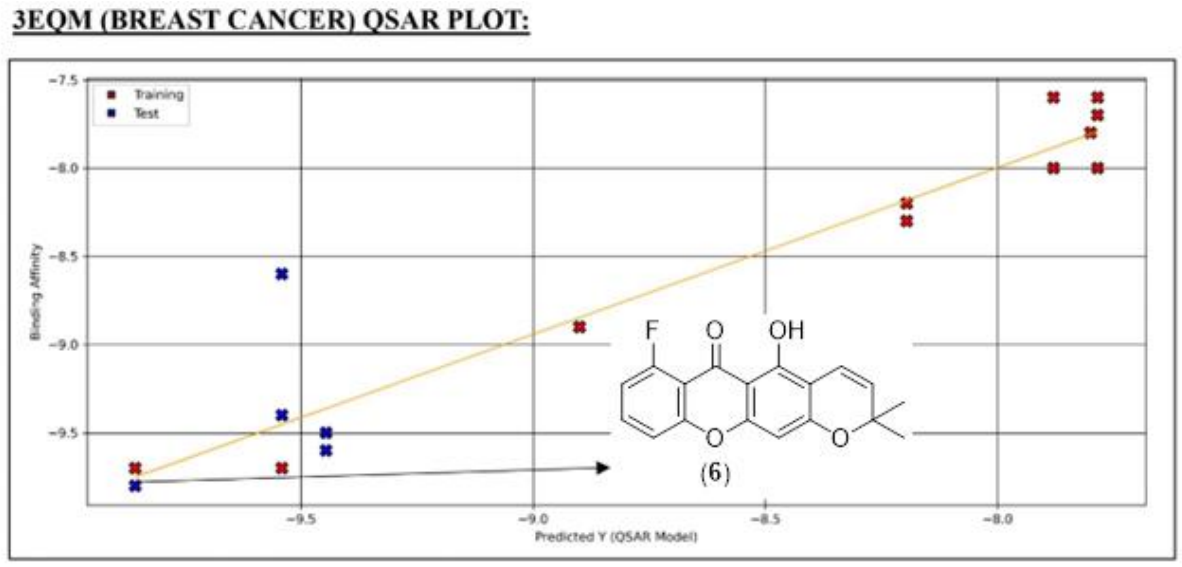

Figure 3. The plots of binding affinity vs predicted Y (QSAR Model). The data for the training set are presented as red crosses, whereas the data for the test set are presented as blue crosses. The yellow line represents the regression line. The QSAR models were constructed with six xanthone derivatives with the aid of ChemMaster 1.1 software.

Table 5. The definition of descriptors for QSAR modelling.

Descriptor Type	**Definition**
Aromatic heavy atom	
Hydrogen-bond (H-bond) acceptors	
Hydrogen-bond (H-bond) donors	Physicochemical Properties
Rotatable bonds	
Molecular weight (MW)	
LogP	Lipophilicity
Lipinski violations	Drug-likeness

Table 6. The equation and predictive performance of the constructed QSAR model for compound **6**.

QSAR Model	**Training set**			**Test set**			**Q^2**
	R^2	**RSME**	**MAE**	**R^2**	**RSME**	**MAE**	
3EQM	0.972	0.131	0.102	-0.102	0.432	0.269	0.926

R^2: Coefficient of determination
RSME: Root mean square error
MAE: Mean absolute error
Q^2: Predictive relevance

Molecular Dynamics

To further support the findings of the QSAR study, a molecular dynamics simulation [48] was performed on the compound **6**-aromatase complex (3EQM). The conformation obtained from the molecular docking study underwent molecular dynamics simulations for 50 ns using AMBER22 software [34]. Analysis of the root mean square displacement (RMSD) of the receptor revealed stabilization after 4 ns, with a consistent trend around 2.5 Å throughout the trajectory (**Figure 4a**). Compound **6** demonstrated stability in the complex from the beginning of the simulation, with the RMSD consistently observed between 0.3-1.3 Å throughout the simulation duration.

To further assess the binding strength of the compound **6**-aromatase complex, the free binding energy was calculated using the MMPBSA method [35]. The total binding energy was determined to be -33.9114 kcal/mol. Additionally, free energy decomposition analysis using the MMPBSA method identified residues CYS437, MET311, ALA306, ALA438, and ALA307 as key contributors, with energy values of -2.273, -1.756, -1.343, -1.334, and -1.267 kcal/mol, respectively (**Figure 4b**).

Further analysis of 2D interactions revealed that CYS437, MET311, ALA306, and ALA307 interacted with compound **6** via hydrophobic interactions, including alkyl-alkyl and π-alkyl, while ALA438 engaged in hydrogen bonding interactions (**Figure 4d**). Analysis of the hydrogen bonding interactions was furthered using the cpptraj program [36], which indicated that interactions between compound **6** and ALA438 were detected throughout 18.54 % of the total simulation duration. Collectively, the findings presented in this study further support the potential inhibition of aromatase by compound **6**.

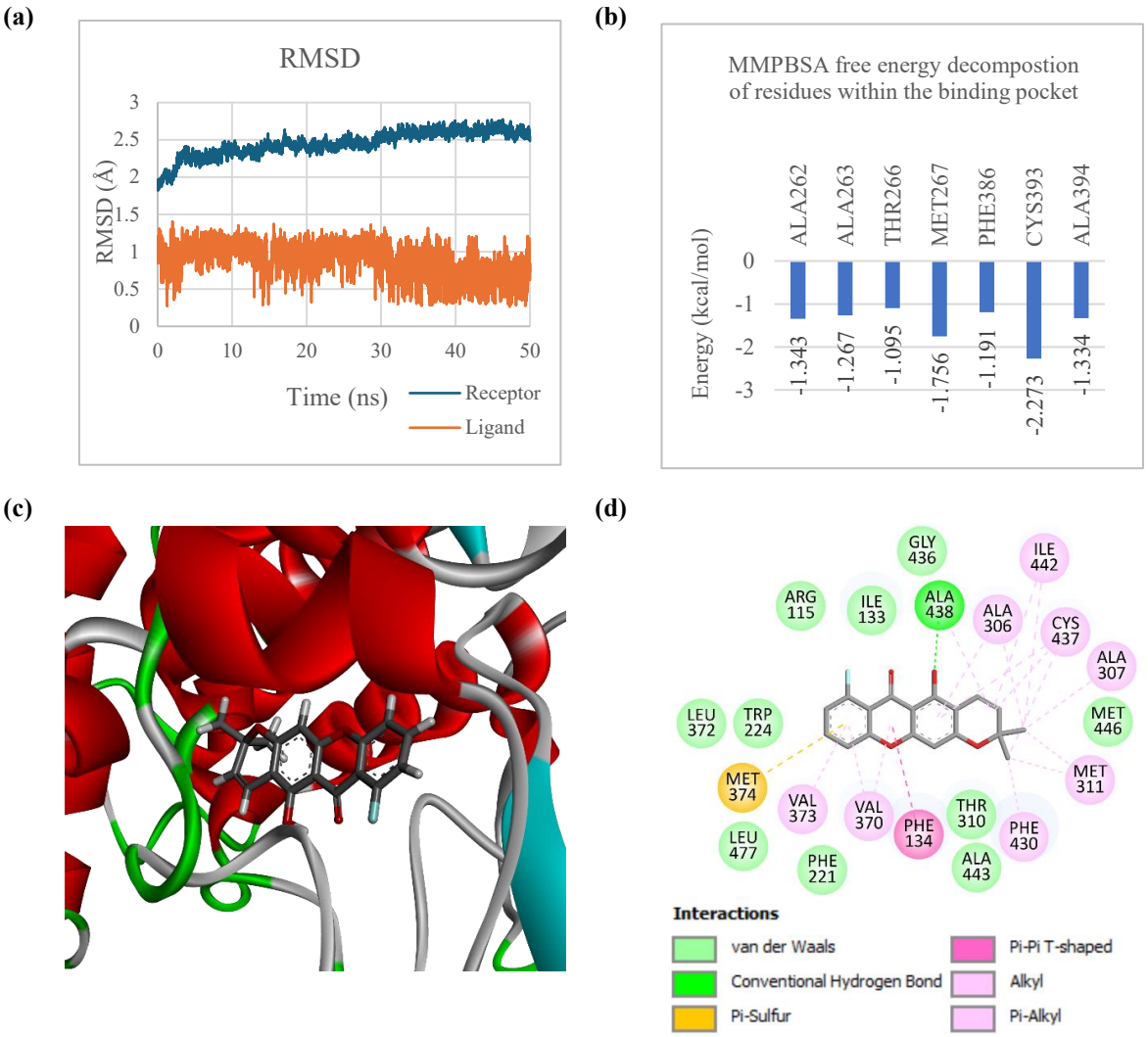

Figure 4. Results of the molecular dynamics simulation of the compound **6**-aromatase complex: **(a)** RMSD of the receptor and ligand; **(b)** Free energy decomposition of residues within the binding pocket; **(c)** 3D diagram of the complex; **(d)** 2D interaction diagram of the complex.

ADMET Property Analysis, Drug-likeness, and Gastrointestinal Absorption and Brain Penetration Prediction [BOILED-Egg] Model.

To identify the toxicity of compound **6,** the ADMET analysis (absorption, distribution, metabolism, excretion, and toxicity analysis) was applied [49]. The predicted pharmacokinetic properties and toxicities included permeability for the blood-brain barrier (BBB), human intestinal absorption (HIA), and P-glycoprotein substrate/inhibitor. Based on the ADMET results in **Table 7**, the negative (-) BBB and HIA permeability indicated that compound **6** was weakly absorbed in the human body [50]. The best-docked molecule (compound **6**) was found to be a P-glycoprotein inhibitor, suggesting that it may interact with other medications or drugs, as drug-drug interactions are initiated by P-glycoproteins [51]. The ADMET analysis also showed that compound **6** was a CYP (human cytochrome P450) enzyme inhibitor, except for isoforms 3A4. Inhibition of CYP enzymes results in either inductive or inhibitory failure of drug metabolism [52] since human cytochrome P450 (CYP) isoforms 1A2, 2C9, 2D6, and 3A4 are responsible for about 90 % of oxidative metabolic activities. The ADMET results also showed that compound **6** was moderately AMES (salmonella/microsome mutagenicity) toxic and noncorrosive to the human eye. Compound **6** was also found to be a weak inhibitor, and inactive towards Human Ether-à-go-go-Related Gene (hERG) inhibition, where hERG is a type of gene sensitive to drug interactions [53]. Thus, compound **6** should bind well with the receptor [54].

Table 7. ADMET properties of compound **6**.

ADMET properties	Value	Outcome
Absorption		
Plasma Protein Binding	97.30 %	High therapeutic index
Blood-Brain Barrier	0.030	BBB-
Human Intestinal Absorption	0.028	HIA-
Caco-2 Permeability	-4.761	Caco2-
P-Glycoprotein Inhibitor	0.997	Inhibitor
P-Glycoprotein Substrate	0.000	Non-substrate
Metabolism		
CYP1A2 inhibitor	0.918	Inhibitor
CYP1A2 substrate	0.677	Substrate
CYP2C19 inhibitor	0.886	Inhibitor
CYP2C19 substrate	0.117	Non-substrate
CYP2C9 inhibitor	0.897	Inhibitor
CYP2C9 substrate	0.933	Substrate
CYP2D6 inhibitor	0.799	Inhibitor
CYP2D6 substrate	0.584	Substrate
CYP3A4 inhibitor	0.492	Non-inhibitor
CYP3A4 substrate	0.155	Non-substrate
Toxicity		
AMES Toxicity	0.633	Moderately toxic
Human Ether-à-go-go-Related Gene Inhibition	0.018	Inactive (Weak inhibitor)
Eye Corrosion	0.005	Noncorrosive

Table 8. The drug-likeness analysis of compound **6**.

Drug-likeness	**Results**
Lipinski	Yes; 0 violations
Ghose	Yes
Veber	Yes
Egan	Yes
Muegge	Yes
Bioavailability Score	0.55

Pharmacokinetics and drug-likeness predictions were also conducted on Lipinski, Ghose, Veber rules and bioavailability scores, as shown in **Table 8**. According to the drug likeness analysis, compound **6** followed and agreed with Lipinski's, Veber's and Ghose's rules because based on the Lipinski's rule (Pfizer's rule, Lipinski's rule of five, RO5), compound **6** did not violate the following properties: MW ≤ 500, Log P ≤ 5, hydrogen bond acceptors ≤ 10, and hydrogen bond donors ≤ 5 [55]. According to Veber's rules, compound **6** had hydrogen bonds ≤ 12, rotatable bonds ≤ 10, and polar surface area (PSA) < 140, with oral bioavailability > 20 % [56]. Additionally, compound **6** had Log P (-0.4-5.6), MR (molar refractivity (40-150), MW (160-480), and the number of atoms (20-70), in agreement with Ghose's rules [57].

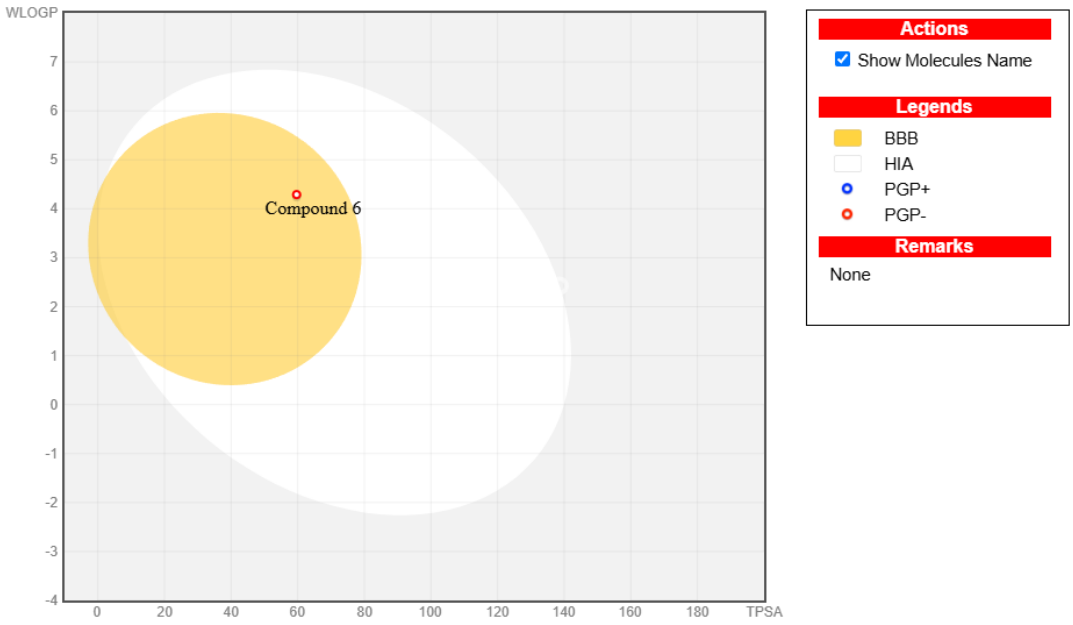

Figure 5. The Brain or Intestinal Estimated permeation method (BOILED-Egg) model.

Pharmacokinetic features were evaluated using the Brain or Intestinal Estimated permeation method (BOILED-Egg), which makes it easier to understand how the molecule's locations in the WLOGP-versus TPSA referential and small molecule lipophilicity and polarity calculations affect the blood-brain barrier (BBB) and passive gastrointestinal tract (HIA), as represented by the yolk and white respectively [39] (**Figure 5**). The findings predict that compound **6** should passively permeate through the blood-brain barrier as it was located in the yolk (yellow) region. This indicates that compound **6** was able to penetrate the central nervous system (CNS) due to its lower molecular weight, moderate lipophilicity and limited polar surface area. Thus, compound **6** exhibited the characteristics of an anti-cancer agent, because the brain is frequently affected by cancer metastases, particularly those that are HER2-positive or triple-negative. The ability of compounds in the yolk region to reach therapeutic quantities in the brain makes them useful for treating these metastases. Additionally, P-glycoprotein plays a key role in limiting the absorption of pharmaceuticals by cells in the brain and the intestinal lumen. This effect is more prominent than its role in promoting drug excretion by hepatocytes and renal tubules into the surrounding luminal space. Therefore, compound **6** was predicted to not be discharged from the central nervous system by the P-glycoprotein [58].

Bioassay

The compounds were studied for their potency against breast cancer cell lines using a screening assay at a concentration of 10 µM. The breast cancer cell line used in this study was MCF-7 (a human breast cancer cell line). The *in vitro* cytotoxicity of compounds **1**–**6** was tested using the MTT assay. Gemcitabine, a chemotherapy drug, was used as a positive control. **Table 9** presents the percentage of cell viability for the compounds at a concentration of 10 µM, where compound **6** was the most potent among them. A compound was considered to have strong activity if the viability of the cells was less than 50 % [22]. To determine the IC_{50} value, compounds **1**–**6** were evaluated at concentrations of 0.1 µM, 1 µM, 10 µM, and 100 µM. Compound **6** exhibited mild activity with an IC_{50} value of 76.94 µM, whereas gemcitabine demonstrated strong activity with an IC_{50} value of 4.0 µM.

Based on the molecular docking, QSAR, and molecular dynamics analyses above, compound **6** was expected to exhibit the most potent effect. However, when we evaluated compound **6** by its effect on cell viability in the MCF-7 cell line and IC_{50}, the results showed that compound **6** exhibited only mild activity against MCF-7 cells. Moreover, its IC_{50} values were significantly higher than those of the standard drug. Although it is not considered cytotoxic toward cancer cells (MCF-7), fortunately, none of the compounds **1**–**6** showed cytotoxicity toward the normal cell line Beas-2B, indicating that these compounds were non-toxic and safe.

Overall, the visual analysis of the new fluorinated xanthone **6** did not correlate with the MTT assay findings. While molecular docking predicted a favourable binding energy of -9.8 kcal/mol for compound **6** compared to the standard at -7.2 kcal/mol, the poor *in vitro* cell viability of compound **6** (92.24 % vs. 22.20 % for the standard) highlights inherent limitations in this computational technique. The accuracy of molecular docking predictions depends on the scoring functions used. Still, these functions do not always capture the full complexity of molecular interactions, sometimes leading to overestimating binding affinity. Furthermore, docking simulations, particularly rigid docking, may neglect crucial conformational changes in the target protein upon ligand binding [59]. Even advanced approaches like flexible and induced-fit docking face challenges in accurately modelling receptor flexibility, which can impact the accuracy of predictions.

In addition, ADMET analysis of compound **6** indicated negative blood-brain barrier (BBB) and human intestinal absorption (HIA) permeability, suggesting weak absorption in the human body. Poor absorption can result in insufficient intracellular concentrations of the compound, thereby reducing its efficacy against target cells [60]. These pharmacokinetic limitations, combined with the possible impact of efflux mechanisms or metabolic instability, could explain why compound **6** failed to demonstrate cytotoxicity in the MCF-7 cell line despite promising in silico findings. This discrepancy underscores the importance of integrating computational modelling with experimental validation, including *in vitro* and pharmacokinetic studies, to accurately assess a compound's therapeutic potential. Ranked binding free energies are not always precise, but they can be used to select new drugs such as small molecules to be experimentally tested in a virtual screening approach.

Table 9. Cell viability of MCF-7 cell lines.

Compounds	Concentration (μM)	Cell Viability (%)	
		MCF-7	Beas-2B
G	10	22.20 ± 1.95	9.64 ± 0.50
1	10	112.92 ± 1.98	91.80 ± 2.17
2	10	114.55 ± 2.02	105.53 ± 2.66
3	10	113.01 ± 1.19	79.87 ± 0.25
4	10	96.70 ± 0.63	84.75 ± 3.16
5	10	99.40 ± 0.15	86.78 ± 1.82
6	10	92.24 ± 1.04	104.13 ± 4.77

***Gemcitabine: standard drug**
***MCF-7: Breast cancer cell line, oestrogen-receptor positive**
***Beas-2B: Non-tumorigenic human lung epithelial cell line**

CONCLUSION

A QSAR study was conducted using ChemMaster 1.1 software to develop models that related the biological activity of derivatives against 3EQM targets. Model stability was assessed through external validation and Y-randomization tests. The QSAR analysis suggests that compound **6**, a newly synthesized fluorinated xanthone, could serve as an effective scaffold for developing novel breast cancer treatments targeting receptor 3EQM, as its Q^2 and R^2 values were close compared to other models. Molecular docking studies were carried out to investigate the ligand-receptor interaction modes and to confirm the stability of the model within the active site. Subsequently, 50 ns MD simulations were performed to estimate the stability of the system under normal physiological conditions, with the highly active compound **6** consistently showing RMSD values of 0.3-1.3 Å. The MTT assay demonstrated that compound **6** was the most effective in inhibiting the human breast cancer cell line, MCF-7. Additionally, compound **6** demonstrated favourable ADMET analysis results.

Compound **6** was found to have a minimal effect on reducing the viability of MCF-7 and exhibited a mild IC_{50} value against MCF-7 breast cancer cells. Despite the strong binding affinity predicted by molecular docking, the compound's poor *in vitro* cytotoxicity highlights the limitations of computational approaches, as scoring functions may overestimate binding affinity and fail to account for receptor flexibility, pharmacokinetics, and cellular uptake barriers. Thus, to fully evaluate compound **6**'s therapeutic potential, future studies should integrate *in vitro* validation, pharmacokinetic assessments, combination therapy strategies, and mechanistic investigations.

ACKNOWLEDGEMENTS

This study was supported by the Ministry of Higher Education Malaysia through the Fundamental Research Grant Scheme (FRGS) with reference code number: FRGS/1/2020/STG04/UPM/02/15. This research was also assisted by Nur Adlina, Jasvinder Kaur Sekhon Sarjeet Singh and Lam Tzi Hui from the University Putra Malaysia (UPM).

REFERENCES

1. Breast cancer [Internet]. [cited 2025 Mac 13]. Available from: https://www.who.int/news/item/01-02-2024-global-cancer-burden-growing-amidst-mounting-need-for-services

2. Łukasiewicz, S., Czeczelewski, M., Forma, A., Baj, J., Sitarz, R. and Stanisławek, A. (2021) Breast Cancer-Epidemiology, Risk Factors, Classification, Prognostic Markers, and Current Treatment Strategies-An Updated Review. *Cancers (Basel)*, **13**, 4287.

3. Li, F. Y., Wang, X., Duan, W. G. and Lin, G. S. (2017) Synthesis and In Vitro Anticancer Activity of Novel Dehydroabietic Acid-Based Acylhydrazones. *Molecules*, **22**, 1087.

4. Seidman, A. (2001) Gemcitabine as single-agent therapy in the management of advanced breast cancer. *Oncology (Williston Park)*, **15**, 11–14.

5. Gemcitabine NDA #200795 (2011).

6. Hao, S., Cai, Z., Zhang, W., Cao, Y. and Du, X. (2022) A convenient synthetic approach to a novel class of aryldifluoromethyl pyrimidine derivatives containing strobilurin motif as insecticidal agents. *J. Heterocycl.Chem.*, **59**, 88–96.

7. Toschi, L., Finocchiaro, G., Bartolini, S., Gioia, V. and Cappuzzo, F. (2005) Role of gemcitabine in cancer therapy. *Future Oncology*, **1**, 7–17.

8. Wang, M. H., Zhang, K. J., Gu, Q. L., Bi, X. L. and Wang, J. X. (2017) Pharmacology of mangostins and their derivatives: A comprehensive review. *Chin. J. Nat. Med.*, **15**, 81–93.

9. Chen, G., Li, Y., Wang, W. and Deng, L. (2018) Bioactivity and pharmacological properties of α-mangostin from the mangosteen fruit: a review. *Expert Opin Ther Pat*, **28**, 415–427.

10. Zhang, H., Tan, Y., Zhao, L., Wang, L., Fu, N. and Zheng, S. (2020) Anticancer activity of dietary xanthone α-mangostin against hepatocellular carcinoma by inhibition of STAT3 signaling via stabilization of SHP1. *Cell Death Dis.*, **11**, 63.

11. Portela, C., Afonso, C. M. M., Pinto, M. M. M., Lopes, D., Nogueira, F. and do Rosário, V. (2007) Synthesis and Antimalarial Properties of New Chloro-9 H -xanthones with an Aminoalkyl Side Chain. *Chem Biodivers*, **4**, 1508–1519.

12. Dolly A. Parasrampuria, Leslie Z. Benet and Amarnath Sharma (2018) Why Drugs Fail in Late Stages of Development: Case Study Analyses from the Last Decade and Recommendations. *The AAPS Journal*, **20**, 46.

13. Pingaew, R., Prachayasittikul, V., Worachartcheewan, A., Thongnum, A., Prachayasittikul, S. and Ruchirawat, S. (2022) Anticancer activity and QSAR study of sulfur-containing thiourea and sulfonamide derivatives. *Heliyon*, **8**, e10067.

14. Cui, W., Aouidate, A., Wang, S., Yu, Q., Li, Y. and Yuan, S. (2020) Discovering Anti-Cancer Drugs via Computational Methods. *Front Pharmacol.*, **11**, 733.

15. Phanus-Umporn, C., Prachayasittikul, V., Nantasenamat, C., Prachayasittikul, S. and Prachayasittikul, V. (2020) QSAR-driven rational design of novel DNA methyltransferase 1 inhibitors. *EXCLI. J.*, **19**, 458–475.

16. Pratiwi, R., Prachayasittikul, V., Prachayasittikul, S. and Nantasenamat, C. (2019) Rational design of novel sirtuin 1 activators via structure-activity insights from application of QSAR modeling. *EXCLI. J.*, **18**, 207–222.

17. Pinto, M. M. M., Sousa, M. E. and Nascimento, M. S. J. (2005) Xanthone Derivatives: New Insights in Biological Activities. *Curr. Med. Chem.*, **12**, 2517–2538.

18. Nguyen, N. T., Nguyen, T. H., Pham, T. N. H., Huy, N. T., Bay, M. Van, Pham, M. Q. (2020) Autodock Vina Adopts More Accurate Binding Poses but Autodock4 Forms Better Binding Affinity. *J. Chem. Inf. Model*, **60**, 204–211.

19. Cooper, G. M. (2024) The Cell. 2000 [cited 2024 Aug 28]; **8**, 103–8. Available from: https://www.ncbi. nlm.nih.gov/books/NBK9839/

20. Pinto, M. and Castanheiro, R. (2009) Synthesis of Prenylated Xanthones: An Overview. *Curr. Org. Chem.*, **13**, 1215–1240.

21. Chang, F. R., Yen, C. T., EI-Shazly, M., Lin, W. H., Yen, M. H. and Lin, K. H. (2012) Anti-Human Coronavirus (anti-HCoV) Triterpenoids from the Leaves of Euphorbia Neriifolia. *Nat. Prod. Commun.*, **7**.

22. Zhou, B. D., Zeng, L. L., Tong, Y. G., Fang, J. Y., Ruan, Z. P. and Zeng, X. Y. (2018) Synthesis and antitumor, antityrosinase, and antioxidant activities of xanthone. *J. Asian Nat. Prod. Res.*, **20**, 467–476.

23. Beidou, Z. (2019) Synthesis and antitumor, anti-tyrosinase, and antiplatelet aggregation activities of xanthone. *Journal of Chinese Pharmaceutical Sciences*, **28**, 247–256.

24. Ghosh, D., Griswold, J., Erman, M. and Pangborn, W. (2009) Structural basis for androgen specificity and oestrogen synthesis in human aromatase. *Nature*, **457**, 219–223.

25. Chen, K., Wang, L., Shen, J., Tsai, A. L., Zhou, M. and Wu, G. (2023) Mechanism of stepwise electron transfer in six-transmembrane epithelial antigen of the prostate (STEAP) 1 and 2. *Elife*, **20**, 12.

26. Martinez-Zapien, D., Ruiz, F. X., Poirson, J., Mitschler, A., Ramirez, J. and Forster, A. (2016) Structure of the E6/E6AP/p53 complex required for HPV-mediated degradation of p53. *Nature*, **529**, 541–545.

27. Rosa, G. P., Palmeira, A., Resende, D. I. S. P., Almeida, I. F., Kane-Pagès, A., Barreto, M. C. (2021) Xanthones for melanogenesis inhibition: Molecular docking and QSAR studies to understand their anti-tyrosinase activity. *Bioorg. Med. Chem.*, **29**, 115873.

28. Trott, O. and Olson, A. J. (2010) AutoDock Vina: Improving the speed and accuracy of docking with a new scoring function, efficient optimization, and multithreading. *J. Comput. Chem.*, **31**, 455–461.

29. Patil, R., Das, S., Stanley, A., Yadav, L., Sudhakar, A. and Varma, A. K. (2010) Optimized Hydrophobic Interactions and Hydrogen Bonding at the

Target-Ligand Interface Leads the Pathways of Drug-Designing. *PLoS One*, **5**, e12029.

30. Hanwell, M. D., Curtis, D. E., Lonie, D. C., Vandermeersch, T., Zurek, E. and Hutchison, G. R. (2012) Avogadro: an advanced semantic chemical editor, visualization, and analysis platform. *J. Cheminform*, **4**, 17.

31. Sheng, Z., Ge, S., Xu, X., Zhang, Y., Wu, P., Zhang, K. (2018) Design, synthesis and evaluation of cinnamic acid ester derivatives as mushroom tyrosinase inhibitors. *Medchemcomm.*, **9**, 853–61.

32. Al-Nema, M., Gaurav, A. and Lee, V. S. (2020) Docking based screening and molecular dynamics simulations to identify potential selective PDE4B inhibitor. *Heliyon*, **6**, e04856.

33. Devakrishnan, P., Nasir, N. M., Stanslas, J., Latif, M. A. M., Ismail, A. Z., Baharuddin, F. F. (2025) Development and Evaluation of selective nitroxanthone Derivatives: A promising compound for Targeting MCF-7 breast cancer cells. *Results Chem.*,**13**, 101998.

34. Case, D. A., Aktulga, H. M., Belfon, K., Cerutti, D. S., Cisneros, G. A., Cruzeiro, V. W. D. (2023) Amber Tools. *J. Chem. Inf. Model*, **63**, 6183–6191.

35. Miller, B. R., McGee, T. D., Swails, J. M., Homeyer, N., Gohlke, H., Roitberg, A. E. (2012) MMPBSA.py: An Efficient Program for End-State Free Energy Calculations. *J. Chem. Theory Comput.*, **8**, 3314–3321, Sep. 11, 2012.

36. Roe, D. R. and Cheatham, T. E. (2013) PTRAJ and CPPTRAJ: Software for Processing and Analysis of Molecular Dynamics Trajectory Data. *J. Chem. Theory Comput.*, **9**, 3084–3095.

37. ADMETlab 2.0 [Internet]. [cited 2024 Aug 30]. Available from: https://admetmesh.scbdd.com/service/screening/cal

38. SwissADME [Internet]. [cited 2024 Aug 30]. Available from: http://www.swissadme.ch/

39. Daina, A., Michielin, O. and Zoete, V. (2017) SwissADME: a free web tool to evaluate pharmacokinetics, drug-likeness and medicinal chemistry friendliness of small molecules. *Sci. Rep.*, **7**, 42717.

40. Indrayanto, G., Putra, G. and Suhud, F. (2021) Validation of in-vitro bioassay methods: Application in herbal drug research. *Profiles of Drug Substances, Excipients and Related Methodology*, **46**, 273–307.

41. Ramakrishnan, S., Nasir, M. N., Stanslas, J., Hamdi, I. F., Mohammad Latif, M. A. and Baharuddin F. F. (2023) One-pot two-component synthesis of halogenated xanthone, 3-o substituted xanthone, and prenylated xanthone derivatives as aromatase inhibitors. *Results Chem.*, **1**, 5.

42. Blakemore, J. and Naftolin, F. (2016) Aromatase: Contributions to Physiology and Disease in Women and Men. *Physiology*, **31**, 258–269.

43. Nabholtz, J. M. (2008) Aromatase inhibitors in the management of early breast cancer. *European Journal of Surgical Oncology (EJSO)*, **34**, 1199–1207.

44. Rocha, S. M., Barroca-Ferreira, J., Passarinha, L. A., Socorro, S. and Maia, C. J. (2021) The Usefulness of STEAP Proteins in Prostate Cancer Clinical Practice. *In: Prostate Cancer. Exon Publications*, 139–154.

45. Jones, L. A., Conway, G. E., Nguyen-Chi, A., Burnell, S., Jenkins, G. J., Conlan, R. S. (2023) Investigating STEAP2 as a potential therapeutic target for the treatment of aggressive prostate cancer. *Cell Mol. Biol.*, **69**, 179–187.

46. Burd, E. M. (2003) Human Papillomavirus and Cervical Cancer. *Clin. Microbiol. Rev.*, **16**, 1–17.

47. Pradhan, S., Mondal, S., Sinha, C. (2016) In search of Tuberculosis drug design: An in-silico approach to azoimidazolyl derivatives as antagonist for Cytochrome P450. *Journal of the Indian Chemical Society*, **93**, 1–18.

48. Tabti, K., Elmchichi, L., Sbai, A., Maghat, H., Bouachrine, M., Lakhlifi, T. (2022) In silico design of novel PIN1 inhibitors by combined of 3D-QSAR, molecular docking, molecular dynamic simulation and ADMET studies. *J. Mol. Struct.*, **1253**, 132291.

49. Lombardo, F., Gifford, E. and Shalaeva, M. (2003) In Silico ADME Prediction: Data, Models, Facts and Myths. *Mini-Reviews in Medicinal Chemistry*, **3**, 861–875.

50. Soga, S., Shirai, H., Kobori, M. and Hirayama, N. (2007) Use of amino acid composition to predict ligand-binding sites. *J. Chem. Inf. Model*, **47**, 400–406.

51. Wang, J., Krudy, G., Hou, T., Zhang, W., Holland, G. and Xu, X. (2007) Development of Reliable Aqueous Solubility Models and Their Application in Druglike Analysis. *J. Chem. Inf. Model*, **47**, 1395–1404.

52. Lin, J. H. and Yamazaki, M. (2003) Role of P-Glycoprotein in Pharmacokinetics. *Clin. Pharmacokinet*, **42**, 59–98.

53. Mortelmans, K. and Zeiger, E. (2000) The Ames Salmonella/microsome mutagenicity assay. *Mutation Research/Fundamental and Molecular Mechanisms of Mutagenesis*, **455**, 29–60.

54. Sanguinetti, M. C. and Tristani-Firouzi, M. (2006) hERG potassium channels and cardiac arrhythmia. *Nature*, **440**, 463–469.

55. Lipinski, C. A., Lombardo, F., Dominy, B. W. and Feeney, P. J. (2001) Experimental and computational approaches to estimate solubility and permeability in drug discovery and development settings. *Adv. Drug Deliv. Rev.*, **46**, 3–26.

56. Veber, D. F., Johnson, S. R., Cheng, H. Y., Smith, B. R., Ward, K. W. and Kopple, K. D. (2002) Molecular Properties That Influence the Oral Bioavailability of Drug Candidates. *J. Med. Chem.*, **45**, 2615–2623.

57. Ghose, A. K., Viswanadhan, V. N. and Wendoloski, J. J. (1999) A Knowledge-Based Approach in Designing Combinatorial or Medicinal Chemistry Libraries for Drug Discovery. 1. A Qualitative and Quantitative Characterization of Known Drug Databases. *J. Comb. Chem*., **1**, 55–68.

58. Shweta, M. and Rashmi, D. (2019) In-vitro ADME studies of TUG-891, a GPR-120 inhibitor using Swiss ADME predictor. *Journal of Drug Delivery and Therapeutics*, **9**, 266–369.

59. Pinzi, L. & Rastelli, G. (2019) Molecular docking: Shifting paradigms in drug discovery. In *International Journal of Molecular Sciences*, **20**, 4331.

60. Klimoszek, D., Jeleń, M., Dołowy, M. & Morak-Młodawska, B. (2024) Study of the Lipophilicity and ADMET Parameters of New Anticancer Diquinothiazines with Pharmacophore Substituents. *Pharmaceuticals*, **17**, 725.